Surface & Coatings Technology xxx (2016) xxx–xxx

Contents lists available at ScienceDirect

Surface & Coatings Technology

journal homepage: www.elsevier.com/locate/surfcoat

Multilayer coatings for Bloch surface wave optical biosensors

P. Munzert [a,*], N. Danz [a], A. Sinibaldi [b], F. Michelotti [b]

[a] Fraunhofer Institute for Applied Optics and Precision Engineering, A.-Einstein-Str. 7, 07745 Jena, Germany
[b] SAPIENZA University of Rome, Basic and Applied Science for Engineering Department (SBAI), Via Antonio Scarpa 16, 00161 Rome, Italy

ARTICLE INFO

Article history:
Received 22 June 2016
Revised 9 August 2016
Accepted in revised form 10 August 2016
Available online xxxx

Keywords:
Optical coating
Polymer
Biosensor
Resonance
Evanescent field

ABSTRACT

Sensors using surface plasmon resonance (SPR) are established as the method of choice in label-free optical biosensing. Their sensitivity for small refractive index changes at the surface originates from the enhanced evanescent field at the surface of a thin metal layer. However, the small number of well-suited metals (Ag, Au) with fixed optical constants limits a further refinement of the SPR performance in terms of dispersion and resonance width. An alternative can be found in Bloch Surface Waves (BSW) sustained at specially designed dielectric multilayer stacks with low absorption losses. Due to the low losses an enormous narrowing of the resonance is obtained, promising the reduction of the detection limit for such a label-free sensor. In order to deposit these multilayers on plastic sensor chips, plasma ion assisted vacuum evaporation (PIAD) was applied as deposition method. SiO_2, TiO_2, and Ta_2O_5 single layer properties were balanced in terms of absorption losses, stability in aqueous environment and film stress. Dielectric multilayer stacks could be designed in a way, that resonance performance is optimal and the total stack thickness as low as possible. Optimized Bloch stacks were successfully coated on a large number of polymer chips. The application could be demonstrated by the detection of cancer biomarkers using an analytical instrument that was developed with the BSW chips as core element.

1. Introduction

The increasing demand for early detection of diseases drives the efforts to develop increasingly sensitive techniques to detect biomarkers in extremely low concentrations. For this, a standard clinical verification method is ELISA [1]. Here a color change reaction of enzyme labeled antibodies takes place, which enables the detection of extremely low concentrations. However, ELISA is rather slow and the reaction kinetics cannot be tracked. An alternative optical biosensing method is surface plasmon resonance (SPR) [2,3] that has evolved to be the standard approach among various label-free optical methods [4]. However, the resonance exploited in plasmon based sensing is governed by the optical properties of the metal film used. The metals of choice are gold or silver; usually only gold is used for practical reasons. This results in missing flexibility in operation wavelength and angle of the resonance peak. Furthermore, the resonance width is determined by the metal losses and cannot be narrowed to lower the limit of detection. A possibility to overcome these drawbacks in optical sensor design is to utilize surface modes at specially tailored dielectric multilayer stacks [5,6]. In such case, called Bloch surface wave, the maximum field intensity is close to the surface of the multilayer stack and an evanescent field extends into the superstrate and is exploited for sensing [7–10]. As appropriate dielectric materials for these multilayers usually exhibit much less absorption than metal films, enormous field enhancement factors associated with potentially very narrow resonances have been observed [11,12]. Advantages of this Bloch surface wave approach in contrast to SPR are that the BSW dispersion can be almost arbitrarily tuned by the stack design and the layer materials used. This means that BSW can operate at any wavelength and the resonance angle can also be adjusted to the sensitivity maximum [13]. Other benefits of the Bloch wave approach come from the fact that the increased surface field enhancement and the absence of the metal layer's quenching can be exploited for fluorescence enhancement of dye molecules at the sensor surface. Compared to conventional fluorescence analysis, where the emission is spread over the whole half-space and only a small amount of the light reaches the detector, the BSW approach allows to concentrate the emission into a small angular range. The emission is not attenuated by metal losses and fluorescence excitation is significantly boosted when performed by the evanescent field of a BSW. Therefore, the new approach is to combine label-free [14] and fluorescence signal detection in only one sensor element [15] that uses such a Bloch multilayer stack. As displayed in Fig. 1, the Kretschmann-Raether configuration with a glass prism [16] is applied but instead of the metal film, which is commonly used for SPR, a dielectric multilayer stack has to be deposited. By illumination with TE polarized light under total internal reflection conditions, a sharp drop in reflectivity appears at the resonance angle when the in-plane propagation constant of the illumination matches

* Corresponding author.
E-mail address: peter.munzert@iof.fraunhofer.de (P. Munzert).

http://dx.doi.org/10.1016/j.surfcoat.2016.08.029
0257-8972/

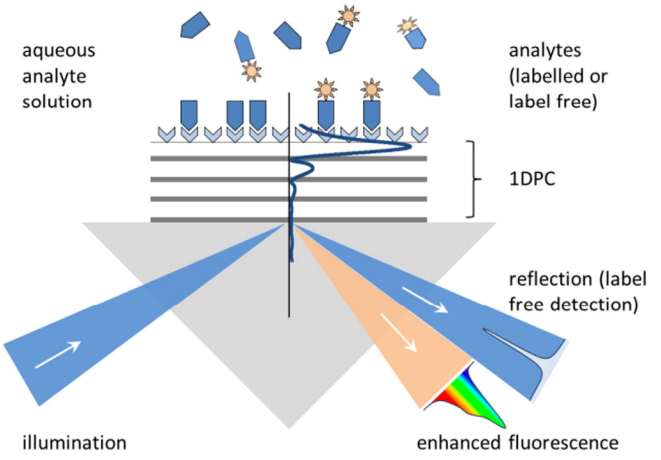

Fig. 1. Scheme of a Bloch surface wave optical biosensor for label-free and fluorescence detection.

that of the surface wave. The reflected light for label-free detection and the spontaneously emitted fluorescence are then observed in the same angular range and can be recorded with the same detector [14].

This paper illustrates the basic principles of BSW generation, the design of dielectric multilayer stacks and the vacuum deposition of these coatings on disposable polymer biochips. With a corresponding sensor chip as core element, an analytical biosensing instrument for the detection of biomarkers is introduced and an actual measurement of the Bloch resonance shift caused by the interaction of biomolecules is shown.

2. Material and methods

Sensor chips with incorporated coupling optics were developed and manufactured from KDS Radeberg by injection molding of a thermoplastic COC polymer (Topas 6013, Topas Advanced Polymers). As coating technology for the deposition of micrometer thick dielectric multilayer stacks on these plastic chips, plasma ion assisted vacuum evaporation (PIAD) with a Bühler/Leybold Optics APS 904 and Syrus Pro 1100 box coaters was applied. This technique allows the deposition of dense coatings without substrate heating, so it is suitable for coating plastics. The film densification was performed by the APS plasma ion source, which emits high energetic Ar-ions during the evaporation process in order to densify the growing film [17]. By varying the ion energy the film densification can easily be adjusted, for example to balance intrinsic film stress. Ion energies of approximately 100 eV were applied for SiO_2 with a deposition rate 0.5 nm/s and for Ta_2O_5 with 0.4 nm/s. For the thin TiO_2 layer 120 eV and 0.25 nm/s were used. Layer thickness termination for the Bloch stacks was primarily done by quartz crystal monitoring. The corresponding calibration factors were derived by ex-situ R/T measurements of single layers having three quarterwaves optical thickness at 550 nm. For advanced experiments, an in-situ optical monitoring system was used for calibrating the quartz crystals in order to lower systematic single layer thicknesses errors. This broad band optical monitoring device OptiMon™ was developed at Fraunhofer IOF [18]. It measures transmittance spectra from samples located on the rotating substrate holder (see Fig. 2) and uses the recalculation routines from the Optilayer™ software in a triangular algorithm [19], allowing one to determine single layer thicknesses inside the stack with a high precision.

Absorption losses for SiO_2 and Ta_2O_5 were determined by laser calorimetry measurements at 1064 nm wavelength performed at Laser Zentrum Hannover (LZH). For ex-situ measurements of transmission and reflection a commercial dual-beam ratio recording spectrophotometer Lambda 900 from Perkin Elmer was used. A special VN-accessory (developed at IOF) enables the absolute measurements of T and R at the same position of the sample surface, avoiding errors due to lateral inhomogeneity or tilt. The beam's angle of incidence is 6° and keeps polarization effects negligible. Refractive indices for the single layers were calculated from the measured R/T spectra in the transparency range, using a simple Cauchy model. A thin film software developed at IOF was applied to calculate resonance properties and to optimize the coating designs. The batch to batch variation of the resonance peak was measured by inserting the coated polymer chips into the analytical instrument and covering them with water. By this system the chip is illuminated by 670 nm emitting laser diode under total internal reflection conditions. The reflected light is detected by a CCD camera for tracking the angular position of the resonance peak.

3. Results and discussion

3.1. Multilayer design for BSW stacks

By the design and the material properties of the multilayer stack, the performance of the resonance peak in terms of dispersion as well as resonance width, depth and shift can be adapted. As the design base for the Bloch stacks a periodic high (H)/low (L) reflector was taken because the light inside the stack has to be optimally reflected to achieve the resonant mode with the light that is totally reflected at the upper boundary. Considering such HL stacks, a common thin film calculation software can indeed calculate the resonance in reflection from a given stack but does not have an efficient reverse simulating option to optimize the

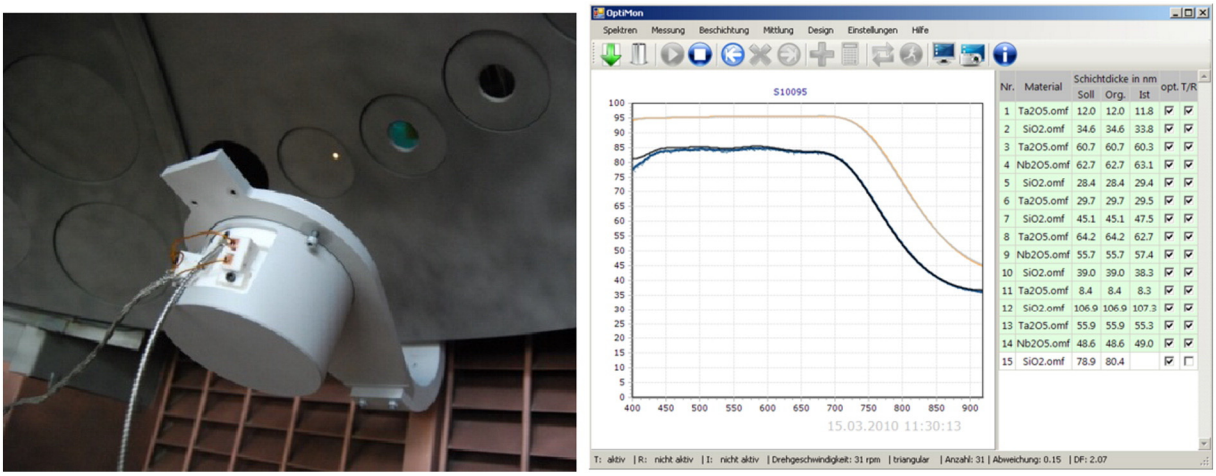

Fig. 2. Optical broadband monitoring system OptiMon™, illumination device mounted in the deposition chamber (left) and graphical user interface (right).

Please cite this article as: P. Munzert, et al., Surf. Coat. Technol. (2016), http://dx.doi.org/10.1016/j.surfcoat.2016.08.029

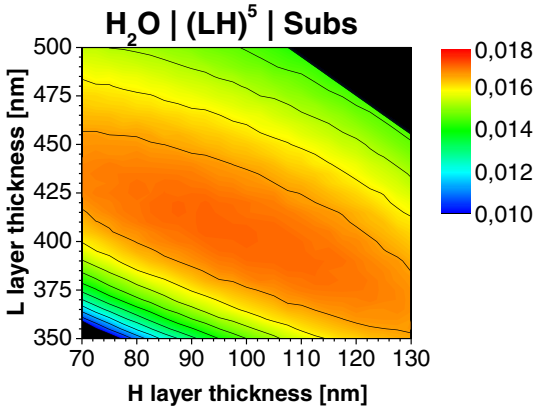

Fig. 3. Sensitivity calculated in terms of angular resonance shift vs. organic adlayer thickness change [°/nm] for a Bloch stack with five periods Ta_2O_5/SiO_2 in dependence of the low and high index layer thicknesses.

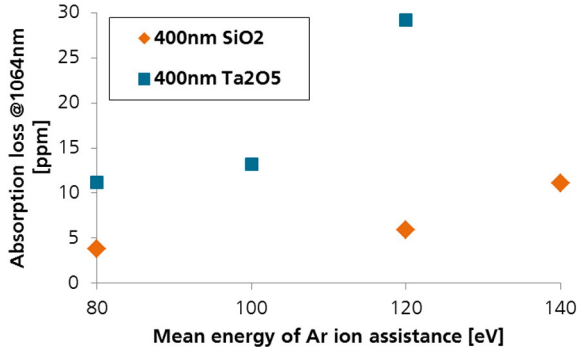

Fig. 5. Experimentally determined losses @1064 nm for SiO_2 and Ta_2O_5 single layers in dependence of the Ar ion assistance energy while deposition.

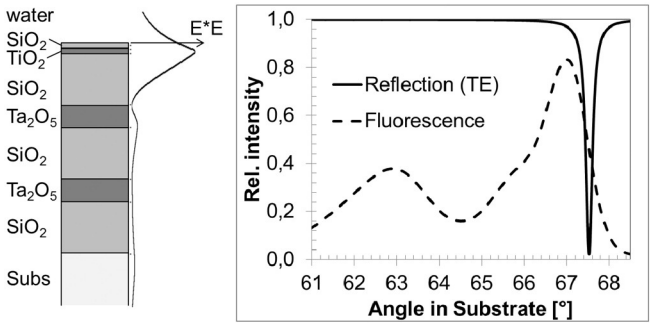

Fig. 6. Optimized stack design with distribution of energy density (left), and simulated angular spectra observed in label-free mode at 670 nm wavelength or in fluorescence mode for the dye DyLight650.

resonance properties. Thus, all resonance properties were calculated in forward direction for a variation of layer thickness combinations and the optimal ranges were taken from these plots. Fig. 3 exemplary illustrates how a suitable thickness combination for the high and low index layers can be determined. The range with maximum sensitivity for this particular stack design can be reached with e.g. 400 nm low index and 100 nm high index material, but layer thickness variation will not affect sensitivity much.

Besides sensitivity, one of the main determining factors for the resonance performance is the absorption loss of the layer materials. As shown in Fig. 4, extremely narrow resonances can be achieved when assuming a material absorption of 3×10^{-6}. Increasing such losses yields considerably broadened resonances.

In PIAD deposition experiments it was possible to minimize material losses by reducing the energy for Ar ion assistance that is applied for the vacuum evaporation process. Fig. 5 shows, that the absorption of a 400 nm thick SiO_2 layer could be reduced to 3 ppm and for Ta_2O_5 down to 12 ppm. These values correspond to $k_{SiO2} \sim 2 \times 10^{-6}$ and $k_{Ta2O5} \sim 1 \times 10^{-5}$, respectively, if an interpolation to the aspired operation wavelength for the analytical instrument of 670 nm is performed.

The number of layer periods in the stack also determines the resonance width and depth depending on the material properties. In our case, two periods yield a too wide and shallow resonance that becomes too narrow for more than four periods. Thus, the optimal number of periods is between three and four, resulting in total thicknesses of these BSW stacks ranging from 1 μm to 2 μm. For the final stack, a non-periodic design was chosen due to a sensitivity for refractive index changes that is three times higher compared to a periodic one. In order to reduce the total thickness of the coating to 1 μm and increase the resonance depth, a 20 nm thin TiO_2 high index layer was set on top of two periods SiO_2/Ta_2O_5 (see Fig. 6).

It is clear that the resonance width was broadened by the elevated losses but limits the propagation length of the surface mode to scales ~100 μm, what is compatible with spot sizes in biochemical sensors.

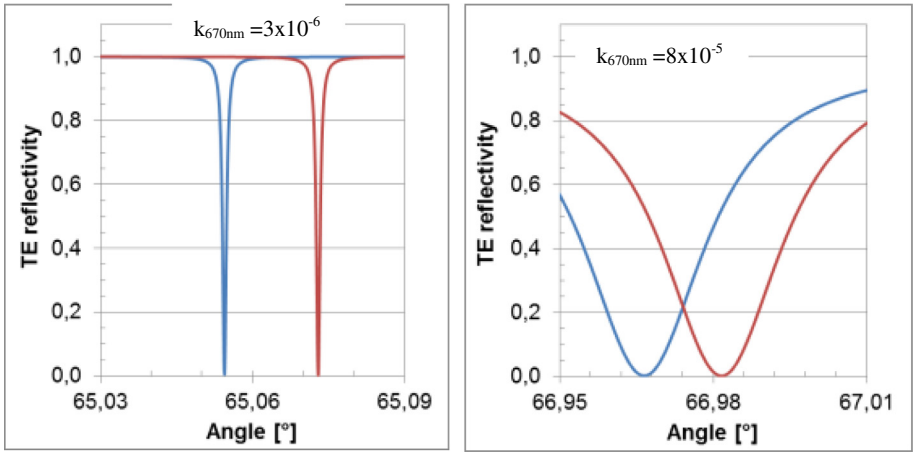

Fig. 4. Optimized reflection resonances for different absorption losses of the dielectric materials in periodic BSW stacks (left: $k_{670\ nm} = 3 \times 10^{-6}$, right: $k_{670\ nm} = 8 \times 10^{-5}$) are shown for two different refractive indices ($n = 1.33$ and $n = 1.34$) of the superstrate to illustrate the resonance shift.

Please cite this article as: P. Munzert, et al., Surf. Coat. Technol. (2016), http://dx.doi.org/10.1016/j.surfcoat.2016.08.029

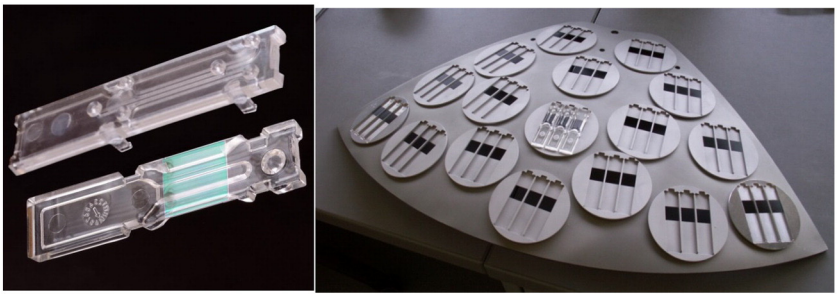

Fig. 7. Polymer chip (coated with a BSW multilayer) with adapter plate for the microfluidic system (left) and APS 904 calotte segment loaded with holders that are adapted to the sensor chip geometry (right).

The uppermost 20 nm thin SiO_2 layer was solely introduced to promote silane coupling for the biochemistry and not for optical reasons. The calculated angular intensity spectra in Fig. 6 illustrate both the monochromatic angular resonance at 670 nm wavelength to be exploited in a SPR-like measurement and the angular dispersion of the fluorescence emitted above 660 nm wavelength in two polarizations. Both modes are covered by one detector and switching the illumination system.

3.2. Bloch stack deposition on plastic sensor chips

The basic idea was to use an injection molded polymer chip where all optical coupling elements are already integrated. In contrast to state-of-the-art glass chips, polymer chips can be manufactured easily and cost effectively in large quantities by injection molding technology, hence the polymer chip can be used as a disposable. Furthermore, the adapter element for microfluidics that enables the analyte solution to reach the chip surface can be adjusted on the chip as a separate click-in element prepared by injection molding as well (see Fig. 7 left). Special substrate holders were developed where only the sensor area of the chip is coated while masking the rest of the chip surface. More than 200 sensor chips could be coated within one batch in an APS 904 box coater although the holders were not optimized with regard to quantity.

Coating experiments were carried out to investigate the adhesion of dielectric layers on the Topas polymer. Tape test revealed that extensive plasma pretreatments are not necessary to promote coating adhesion. Thus, only a short pre-etching step with the APS source at 80 eV for 60 s pure argon plasma was sufficient. With regard to the film properties, an adjustment of layer densification was necessary. Highly densified PVD coatings exhibit considerable compressive stress which results in huge interface forces on the polymer substrate if the coating is thick. Due to the difference in thermal expansion coefficients between the organic substrate and the inorganic coating, the temperature rise during the deposition is an additional component that introduces interface forces. If the APS source operates in the upper ion energy mode, a high thermal impact on the substrates can be observed. By lowering ion energies, the thermal load can be reduced. Therefore, less densification was applied for the BSW stack deposition to reduce not only the internal film stress, but also the heat impact on the substrate. Besides this, absorption losses are also lower for less densified coatings as already shown in Fig. 5.

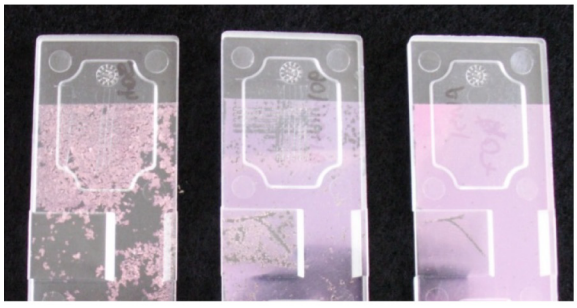

layer densification	film stress [Mpa]	coating delamination after water storage
low	-163.20 compressive	>70%
medium	-277.70 compressive	5 - 10%
high	-382.00 compressive	<5%

Fig. 8. Coating performance after three days' water storage for multilayer coatings with different densification and corresponding film stress values.

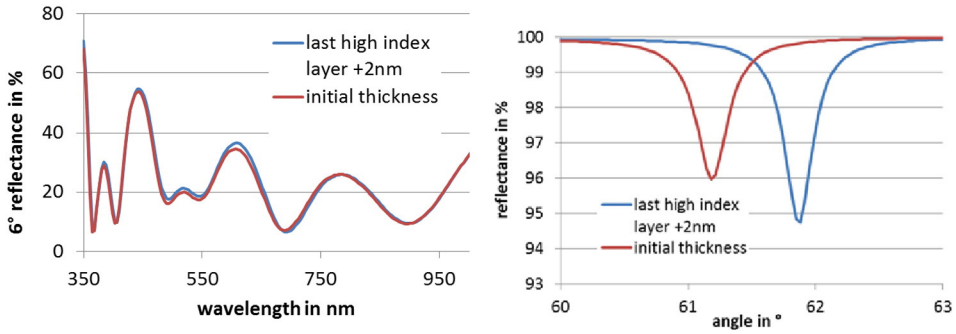

Fig. 9. Calculated 6° reflectance spectrum (left) and resonance peak obtained under total reflectance (right) for the optimized Bloch stack design and a +2 nm thickness variation of the last high index layer.

Please cite this article as: P. Munzert, et al., Surf. Coat. Technol. (2016), http://dx.doi.org/10.1016/j.surfcoat.2016.08.029

Table 1
Single layer thicknesses for a typical Bloch stack; target thicknesses derived from the calculated design and actual thicknesses determined by the BBM after proper calibration of the quartz crystals.

Layer no.	Material	Target thickness	Actual thickness
1	SiO_2	340.0 nm	334.7 nm
2	Ta_2O_5	120.0 nm	120.6 nm
3	SiO_2	340.0 nm	335.6 nm
4	Ta_2O_5	120.0 nm	120.3 nm
5	SiO_2	340.0 nm	341.7 nm
6	Ta_2O_5	120.0 nm	118.8 nm
7	SiO_2	340.0 nm	343.2 nm
8	Ta_2O_5	20.0 nm	19.2 nm
9	SiO_2	20.0 nm	18.6 nm

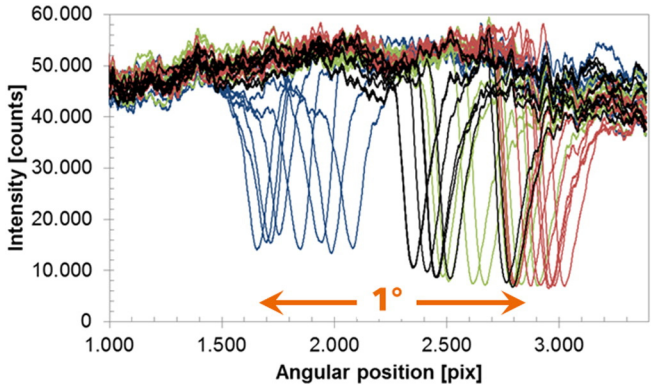

Fig. 10. Deviation of the measured resonance peak position for 4 consecutive coating batches each with 8 chips.

Working with the sensor chips in an aqueous environment resulted in a temporal shift of the resonance peak due to water penetration into the stack. This highly undesired behavior limits measurements in biosensing experiments, as the chip itself causes the same shift of the resonance as a biochemical reaction. It would therefore falsify the verification results. Moreover, the porous coating started to delaminate after three days storage in water as shown in Fig. 8. However, it has to be noted that these chips should be used as disposable sensors and the coating has to be stable only for the time the chip is in use. Therefore, the densification was optimized both with respect to the delamination problem as well as to keep film stress and optical losses as low as possible.

3.3. Reliability of the BSW multilayer deposition

Quartz crystal monitoring (QCM) was used for termination of the single layer thicknesses inside the stack. Usually, the QCM is calibrated from a recalculation of layer thicknesses in the stack using a 0° or 45° ex situ reflectance measurement. However, in the case of Bloch stacks, a deviation in layers where the field intensity is concentrated has a huge effect on the resonance angle measured in total reflectance (see Fig. 9, right diagram). Unfortunately, only a minor effect of such variations is observable for the 0° or 45° reflectance curve. This introduces a systematic error for the thickness calibration.

To minimize systematic thickness errors that originate from insufficient calibration of the quartz crystal monitor, coating deposition runs with in-situ broad band optical monitoring (BBM) were performed. From preliminary experiments, where all layers inside a BSW stack were terminated by quartz crystal monitoring but the optical monitor was activated simultaneously, it was possible to adjust thickness calibration factors correctly. Finally, a Bloch stack with nine layers, including layers with a thickness from 20 nm up to 340 nm from the same material, could be deposited with a precision better than 1.5% for the thick layers and better than 1.5 nm for the thin layers (Table 1).

In addition, layer thickness random errors were in the range of 3% because of non-perfect coating densification and a resulting vacuum to air shift. By a measurement of the resonance peak position for multiple chips from four consecutive coating runs it was found that the variation between single batches added to the variation within a batch amounts to approximately 1° (see Fig. 10). This range must be considered as the minimal angular detection range for the analytical instrument.

3.4. Analytical instrument/measurement of small biomarker concentrations

The basic concept for the analytical instrument was to combine label-free and fluorescence mode using the same detector unit. In the label free mode the sensor chip is illuminated from the rear side by TE polarized light of a 670 nm laser diode. The light is totally reflected at the upper chip surface and directed by some imaging optics to a CCD array. There, the resonance peak that is a dip in reflectance and appears as a narrow dark line on the CCD image (see Fig. 11 left). The position of the resonance is tracked over time, and changes are interpreted as binding or dissociation events at the sensor surface. Thanks to the purposely designed optical system [15], different locations on the chip surface can be analyzed simultaneously. In the fluorescence mode, another light

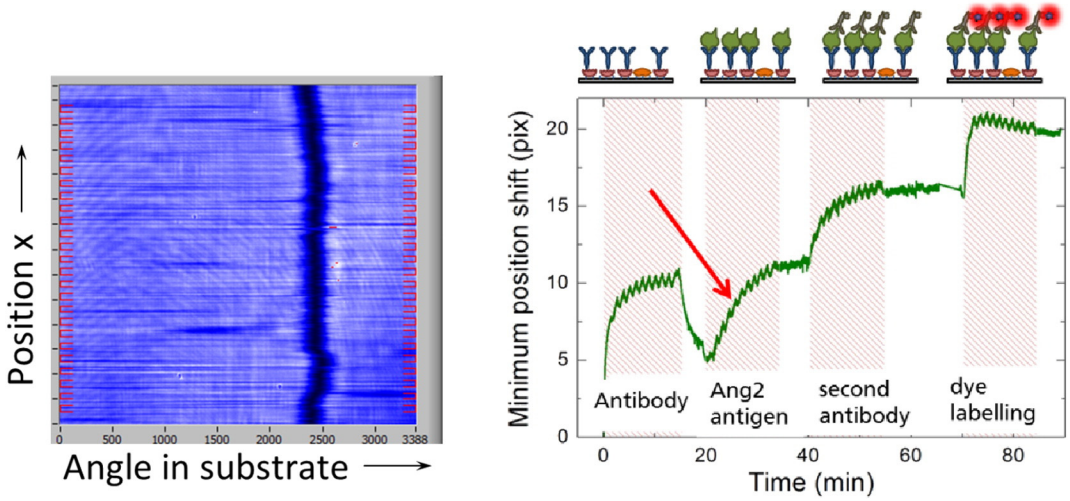

Fig. 11. Example of a CCD image obtained in label-free detection modes (left) and measured resonance shift for an Antigen (Angiopoietin2) – Antibody coupling reaction taking place in the time interval t∈(20 min, 40 min). (right). The resonance shifts observed for $t > 40$ min are due to the injection of biotinylated detection antibody (second antibody) and dye labeled neutravidin solutions that are used to label the chip for the fluorescence part of the assay (not reported here).

Please cite this article as: P. Munzert, et al., Surf. Coat. Technol. (2016), http://dx.doi.org/10.1016/j.surfcoat.2016.08.029

source is used for excitation of a fluorescence dye, but the whole detection optics remains the same. The fluorescence evaluation is performed by a wavelength resolved observation of emission intensity changes.

A label-free measurement of the Angiopoietin 2 cancer biomarker was performed by an Angiopoietin 2/antibody coupling reaction. Therefore different analytes had to be flown over the chip surface by means of a purposely developed microfluidic system. The diagram in Fig. 11 (right) shows the resonance peak shift over time and illustrates the different steps of such initial experiment that were necessary for verification purposes. The curve was normalized by subtracting the signal measured in a reference spot that was blocked with bovine serum albumin. Thereby, the decisive peak shift (marked with the arrow) appeared for the case of the specific binding reaction between the antigen in solution, with a concentration 20 nM, to its antibody that was previously bound onto the sensor surface. This shift reduces with decreasing Angiopoietin 2 concentration. Therefore, as long as this shift is still distinguishable from the measurement noise an even smaller concentration can be detected which is the final objective e.g. in early cancer diagnosis.

4. Conclusions

A special application for dielectric optical interference coatings was illustrated. In contrast to most optical multilayers where reflectance or transmittance towards air is exploited, stacks for the generation of Bloch Surface Waves (BSW) operate in total internal reflection conditions with the objective of generating an evanescent field on top of the uppermost layer. We were able to demonstrate that the successful deposition of such multilayer stacks on plastic substrates is possible by plasma ion assisted vacuum evaporation (PIAD). Due to the high thickness and refractive index precision on a large area, the flexibility in the densification of the layers and in the adjustment of absorption losses, the PIAD deposition method is well suited for this kind of multilayer coatings. Taking into account the size of a typical evaporation box coater, more than 500 polymer chips could be coated within one single deposition run if the substrate holder configuration is optimal. By the coating design and the properties of the dielectric layer materials it was possible to tailor the evolving resonance peak in terms of width, depth and dispersion. This adjustability is a clear benefit compared to Surface Plasmon Resonance (SPR) which represents one of the standard optical biosensing methods and works with a thin metal layer whose optical properties restrict the resonance performance. Through an appropriate design of single layer thicknesses inside a BSW stack e.g. the resonance angle can be tuned for a wide range of operation wavelengths. Therefore, the application of such a sensor would also be possible in the UV or IR. Suitable coating materials with low losses in a wide UV and IR range are state of the art for vacuum evaporation and could be applied for such specially designed Bloch multilayer stacks without major difficulties.

Acknowledgements

This research was funded by the European Commission through the project BILOBA (Grant agreement 318035). The authors acknowledge the collaboration with all other partners of the BILOBA project, in particular with Riccardo Rizzo who contributed to the design of the photonic crystals.

References

[1] R. Lequin, Enzyme immunoassay (EIA)/enzyme-linked immunosorbent assay (ELISA), Clin. Chem. 51 (12) (2005) 2415–2418.
[2] J. Homola, Surface plasmon resonance sensors for detection of chemical and biological species, Chem. Rev. 108 (2008) 462–493.
[3] J. Homola, S.S. Yee, G. Gauglitz, Surface plasmon resonance sensors: review, Sensors Actuators B 54 (1999) 3–15.
[4] C. Ciminelli, C.M. Campanella, F. Dell'Olio, C.E. Campanella, M.N. Armenise, Label-free optical resonant sensors for biochemical applications, Prog. Quant. Electron. 37 (2013) 51–107.
[5] M. Shinn, W.M. Robertson, Surface plasmon-like sensor based on surface electromagnetic waves in a photonic crystal, Sensors Actuators B 105 (2005) 360–364.
[6] P. Yeh, A. Yariv, C.-S. Hong, Electromagnetic propagation in periodic stratified media. I. General theory, J. Opt. Soc. Am. 67 (1977) 423–438.
[7] V.N. Konopsky, E.V. Alieva, Photonic crystal surface waves for optical biosensors, Anal. Chem. 79 (2007) 4729–4735.
[8] F. Giorgis, E. Descrovi, C. Summonte, L. Dominici, F. Michelotti, Experimental determination of the sensitivity of Bloch Surface Waves based sensors, Opt. Express 18 (2010) 8087–8093.
[9] V.N. Konopsky, T. Karakouz, E.V. Alieva, C. Vicario, S.K. Sekatskii, G. Dietler, Photonic crystal biosensor based on optical surface waves, Sensors 13 (2013) 2566–2578.
[10] A. Sinibaldi, R. Rizzo, G. Figliozzi, E. Descrovi, N. Danz, P. Munzert, A. Anopchenko, F. Michelotti, A full ellipsometric approach to optical sensing with Bloch surface waves on photonic crystals, Opt. Express 21 (2013) 23331–23344.
[11] C. Ndiaye, M. Zerrad, A.L. Lereu, R. Roche, P. Dumas, F. Lemarchand, C. Amra, Giant optical field enhancement in multi-dielectric stacks by photon scanning tunneling microscopy, Appl. Phys. Lett. 103 (2013) 131102.
[12] A. Sinibaldi, N. Danz, E. Descrovi, P. Munzert, U. Schulz, F. Sonntag, L. Dominici, F. Michelotti, Direct comparison of the performance of Bloch surface wave and surface plasmon polariton sensors, Sensors Actuators B 174 (2012) 292–298.
[13] R. Rizzo, N. Danz, F. Michelotti, E. Maillart, A. Anopchenko, C. Wächter, Optimization of angularly resolved Bloch surface wave biosensors, Opt. Express 22 (19) (2014) 23202.
[14] N. Danz, A. Kick, F. Sonntag, S. Schmieder, B. Höfer, U. Klotzbach, M. Mertig, Surface plasmon resonance platform technology for multi-parameter analyses on polymer chips, Eng. Life Sci. 11 (6) (2011) 566–572.
[15] N. Danz, A. Sinibaldi, P. Munzert, A. Anopchenko, E. Förster, S. Schmieder, R. Chandrawati, R. Rizzo, R. Heller, F. Sonntag, A. Mascioletti, S. Rana, T. Schubert, M. Stevens, F. Michelotti, Biosensing platform combining label-free and labelled analysis using Bloch surface waves, Proc. SPIE 9506 (2015) 95060V.
[16] H. Raether, Surface Plasmons, in: G. Höhler (Ed.) Springer Tracts in Modern Physics, vol. 111, Springer, Berlin, 1988.
[17] S. Pongratz, A. Zöller, Plasma ion assisted deposition: a promising technique for optical coatings, J. Vac. Sci. Technol. A 10 (1992) 1897–1904.
[18] S. Wilbrandt, O. Stenzel, N. Kaiser, M.K. Trubetskov, A.V. Tikhonravov, In situ optical characterization and reengineering of interference coatings, Appl. Opt. 47 (13) (2008) C49–C54.
[19] A.V. Tikhonravov, M.K. Trubetskov, Online characterization and reoptimization of optical coatings, Proc. SPIE 5250 (2003) 406–413.

Please cite this article as: P. Munzert, et al., Surf. Coat. Technol. (2016), http://dx.doi.org/10.1016/j.surfcoat.2016.08.029